Journal of Building Performance Simulation

ISSN: 1940-1493 (Print) 1940-1507 (Online) Journal homepage: https://www.tandfonline.com/loi/tbps20

A new local pressure loss coefficient model of a duct tee junction applied during transient simulation of a HVAC air-side system

Qiujian Wang, Yiqun Pan, Mingya Zhu, Zhizhong Huang & Peng Xu

To cite this article: Qiujian Wang, Yiqun Pan, Mingya Zhu, Zhizhong Huang & Peng Xu (2018) A new local pressure loss coefficient model of a duct tee junction applied during transient simulation of a HVAC air-side system, Journal of Building Performance Simulation, 11:1, 113-127, DOI: 10.1080/19401493.2017.1288762

To link to this article: https://doi.org/10.1080/19401493.2017.1288762

Published online: 17 Feb 2017.

Journal of Building Performance Simulation, 2018
Vol. 11, No. 1, 113–127, http://dx.doi.org/10.1080/19401493.2017.1288762

A new local pressure loss coefficient model of a duct tee junction applied during transient simulation of a HVAC air-side system

Qiujian Wang[a], Yiqun Pan[a]*, Mingya Zhu[a], Zhizhong Huang[b] and Peng Xu[a]

[a]*School of Mechanical Engineering, Tongji University, Shanghai, China;* [b]*Sino-German College of Applied Sciences, Tongji University, Shanghai, China*

(*Received 12 September 2016; accepted 26 January 2017*)

Most of the local pressure loss coefficient (LPLC) models for duct fittings used in heating, ventilation and air conditioning (HVAC) air-side system transient simulations are simplified. The LPLCs are defined as having a constant value at the rated flow condition or as having a polynomial function of the flow ratio (or velocity ratio). To determine the influence of these simplifications, this study used a diverging tee junction as an example. First, we performed CFD calculations to generate a new LPLC dataset and trained a data-driven model using feature weighted support vector regression (FWSVR) combined with particle swarm optimization (PSO-FWSVR). Finally, we compared this new LPLC model with the two traditional models at the level of both individual junction and air-side system. The results show that the accuracy of the new model is greatly improved and the LPLC model can have a significant impact on the system operation condition.

Keywords: HVAC air-side system; system pressure-and-flow coupling; local pressure loss coefficient; uniform design; feature weighted SVR

Introduction

Indoor comfort with low energy consumption is always the common goal of heating, ventilation and air conditioning (HVAC) engineers. Among the main subsystems of a HVAC system, the air-side system controls the amount of energy that is transmitted into the occupied space and it has the most direct influence on the indoor environment. A well-controlled air-side system is beneficial to achieving this goal. To test the effectivity of a new control strategy, simulation is often used. There are several commonly used HVAC transient simulation platforms, such as TRNSYS, Simulink and Dymola. Researchers use these platforms to reflect the variation of the operational system condition, for example, how the supply air flow varies when adjusting the openings of terminal dampers. When conducting a transient simulation of the air-side HVAC system, the balance between fan pressure and ductwork resistance should be considered carefully. This balance will determine the flow condition of the air distribution system, including the total air flow rate (FR) and flow allocation among the air branches and, finally, the temperature of every single terminal zone supplied by one air branch. As a result, the resistance property of the component models is important for correct simulation of a HVAC air-side system. However, the resistance properties of duct fittings are often neglected or greatly simplified. Besides control simulation, many energy analysis programmes use correlation-based models that relate the part-load supply air FR with the part-load fan electric demand with the neglection of duct resistance property. It is a simplified and computationally efficient way. But considerable errors are inevitable if high precision of simulation for control is required for one's research purpose.

Chen and Treado (2014) developed a Simulink block library of dynamic HVAC component models, in which the modules of junctions, such as flow splitting and merging, are included. The pressure loss at these junctions is defined as the product of a constant value and the square of the mass FR of air, as Equation (1) for splitting. The same constant value assumption is also adopted by the Modelica Building Library (Wetter 2009), as Equation (2), which was developed by LBNL. With regards to TRNSYS, the flow split type in its official type library does not contain resistance properties. As a result, some researchers have developed their own fitting types. Liu, Peng and Zhang (2012) built a mathematical model to reflect the hydraulic characteristics of a VAV (variable air volume) air-side system and defined the local pressure loss coefficient (LPLC) of a tee junction as a quadratic polynomial function of the flow ratio of the downstream branch to the upstream branch, as Equation (3). These references present two LPLC models for tee junctions, with different degrees of simplification, that is, a constant value model and a polynomial model. One question that arises: How will these

*Corresponding author. Email: yiqunpan@tongji.edu.cn

two models function in simulating the real-time operational condition of the air-side system? Will the simplification applied to models have any influence on the accuracy of the simulation?

$$\Delta p = 0.5Ksign(m_i)m_i^2 + 0.5Ksign(m_o)m_o^2, \quad (1)$$

$$\Delta p = \frac{m^2}{(m_{nominal}/\sqrt{\Delta p_{nominal}})^2}, \quad (2)$$

$$\Delta p = a \cdot \mathrm{FR}^2 + b \cdot \mathrm{FR} + c, \quad (3)$$

where m is the mass flow rate (kg/s), FR is the flow rate ratio between downstream and upstream branch; the subscripts of i and o mean inlet and outlet branches, and *nominal* means the value under nominal conditions.

If one wants to build a new fitting resistance model or select proper parameters for known models, the existing LPLC tables are a fundamental dataset that can be used. The LPLC of duct fitting is a historical research topic dating back to the 1950s. Most of the early studies were experimentally based, including the works of ASHRAE (2009), Miller (1971), Idel'chik (1986). However, since the experimental method and the geometry details for a type of fitting, such as a tee junction, are different from each other, there are differences among the LPLC results from different experiments. The results from the former Soviet Union were used in China until the 1980s, when the China Ministry of Construction organized a series of studies to construct an internal LPLC database and eventually published a handbook (China Academy of Building Research 1978) of ducts and fittings. For only three-way junctions, the handbook gives seven recommendations for geometric configurations and also tables of LPLCs for different combinations of ARs and FRs for the branch section to the upstream section for each configuration. The LPLC tables for many types of fittings can also be found in the chapter on duct design in the ASHRAE Handbook of Fundamentals (2009). However, Shao and Riffat (1995) stated that some of the LPLCs for junctions in the ASHRAE handbook may have large errors due to neglecting the Reynolds number.

CFD has proved to be convenient and sufficiently accurate to calculate LPLCs for duct fittings and has been used since the end of the last century. Mumma, Mahank and Ke applied the k–ε model to determine the LPLC of a flat oval duct (1997) and fittings (1998) and compared the prediction results to the measured data. Gan and Riffat (2000) obtained LPLCs for a square cross section junction in converging and diverging conditions with various flow ratios. The CFD results exhibit good agreement with the measured data. They also used a polynomial function to describe the relationship between the junction LPLC and flow ratios. To generalize the use of CFD in LPLC calculations, ASHRAE organized an international competition for predicting LPLCs of a duct junction using CFD without previous knowledge of the experimental data. The winner of this contest, Liu, Long, and Chen (2012), described the entire process for numerical calculation and comprehensively analysed the influence of the mesh size, turbulence model and surface roughness. They emphasized that surface roughness has a great impact on the performance of CFD when determining LPLCs.

From all of the existing LPLC datasets and the related literature, we know that LPLC is mainly affected by geometry factors, the real-time flow allocation and upstream flow condition. An ideal LPLC model should be capable of simultaneously reflecting the influence of all of these factors. In the meantime, the model should be easy to use and run quickly. The geometry parameters are set by users prior to the simulation, and the flow condition variables are transmitted among different modules during simulation. Unfortunately, this type of model is not found in any available relevant studies.

Therefore, in this study, we examined a diverging smooth tee junction as an example to describe the process for new LPLC model development. Then, the proposed model was compared to two simplified LPLC models (polynomial and constant value model) to validate the improved accuracy and determine the error from the junction resistance simplifications.

Methodology

Since the existing LPLC database may have some flaws, we had to generate a new set of LPLC data. We chose to use CFD to calculate the LPLCs of the objective junctions since it is more economical than determining them experimentally. According to Liu, Long, and Chen (2012), the surface roughness has a significant influence on the CFD results for the LPLC. Therefore, it is necessary to first calibrate the relevant CFD parameter settings. We performed a small fraction of the experiments on an individual diverging tee junction to calibrate the relevant parameters in the CFD settings and assumed that the calibrated parameter combination was applicable throughout the subsequent CFD cases, since the material and manufactural specification of the ducts and junctions is the same. Once the CFD parameters are calibrated, the LPLC results from these CFD calculations were used as the dataset.

Then, we designed cases for the CFD calculations so that the junction geometry and flow condition factors could be considered simultaneously. Orthogonal design and uniform design are two commonly used experimental design methods. Considering the time required for CFD, reducing the number of cases becomes the first priority when choosing the case design method. Comparatively speaking, a uniform design can arrange more levels of independent variables under the same number of tests with better sampling uniformity. Fang et al. (2000) proposed this method and applied it broadly in many fields (Fang et al. 2000; Fang and Lin 2008). Therefore, we adopted the uniform design method in this work.

During the model fitting procedure, response surface and machine learning methods are commonly used. From observing the existing LPLC data, the relationship between the LPLC and geometry and flow condition factors is quite nonlinear. In addition, since generating the training dataset for the LPLC is very time-consuming, even for CFD, the size of the dataset cannot be large. Therefore, we chose the support vector regression method (SVR) proposed by Vapnik (1995) to fit the LPLC data, as it has a good generalization performance and predictive accuracy in regard to dealing with a small sample size, nonlinearization and a high number of dimensions. Using previous research (Lin et al. 2008; Niu and Guo 2010), we utilized the particle swarm optimization (PSO) algorithm to optimize the SVR parameter and also the weight factors for different independent variable features to improve the predictive performance.

Finally, we compared this new LPLC model with the two traditional models in two stages. During the first stage, we compared the LPLC results from the PSO-FWSVR model with those from the polynomial function model on the same test dataset to determine the deviation in the LPLC for an individual junction. Second, we built a simple ductwork system to demonstrate the influence of the three different LPLC models on the simulated results for the system operation conditions at the system level. The entire workflow is shown in Figure 1.

Tee junction resistance experiment and CFD parameter calibration

The item chosen for examination in this work is a smooth duct tee junction, as shown in Figure 2. The duct was made from galvanized iron sheet and connected by a flange with a foam stripe added to seal the connection. Figure 3 shows that the length of the straight duct upstream and downstream of the junction was set to 11.5D and 16D, respectively, according to ASHRAE Standard 120 (ASHRAE, 2008), where D is the hydraulic diameter. The position of the pressure measuring section was set to 1.5D upstream from the junction inlet and 12D downstream from

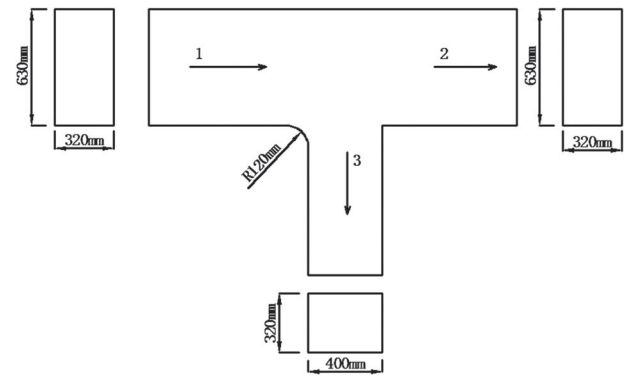

Figure 2. Diagrammatic drawing of experimental tee junction with cross sections.

the two outlets. The FR was measured prior to entering the upstream duct and after exiting the downstream duct. The air FR of the blower was controlled according to the difference between measured the upstream FR and its set-point at a precision of $\pm 3\%$. Flow allocation between the two branches was achieved by changing the position of the dampers attached to the end of each branch. During the experimental process, the total flow was set at five levels, evenly spaced from 3277 to 4865 m^3/h. For each level of total flow, the vertical branch flow was adjusted at five levels that were evenly spaced from 290 to 2080 m^3/h. There were $5 \times 5 = 25$ cases for each branch.

LPLC was calculated using the following equations, referenced from ASHARE handbook (2009) and Standard 120 (2008).

For blow-through branch:

$$\xi_b = \frac{(1/2\rho V_u^2 + P_{s,u}) - (1/2\rho V_b^2 + P_{s,b}) - \Delta P_{f,u} - \Delta P_{f,b}}{1/2\rho V_u^2}. \tag{4}$$

For vertical branch:

$$\xi_v = \frac{(1/2\rho V_u^2 + P_{s,u}) - (1/2\rho V_v^2 + P_{s,v}) - \Delta P_{f,u} - \Delta P_{f,v}}{1/2\rho V_u^2}. \tag{5}$$

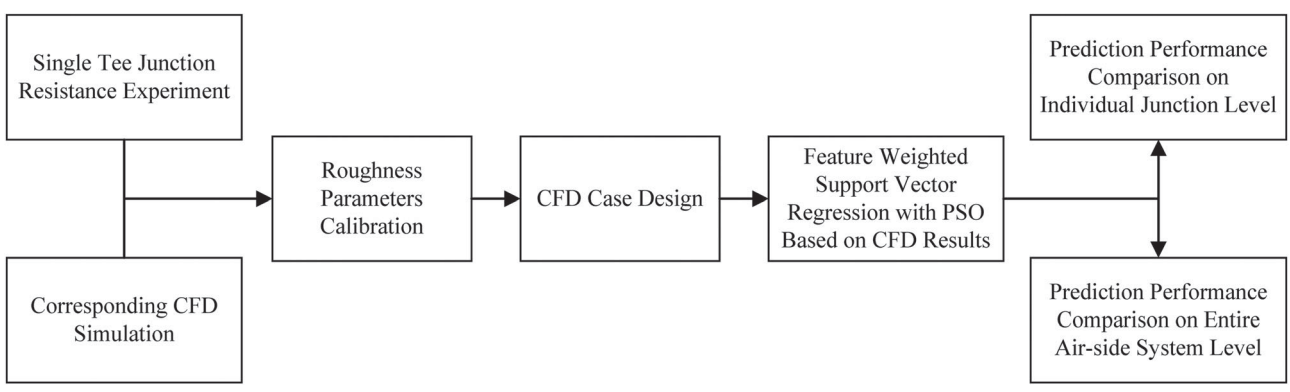

Figure 1. Workflow diagram.

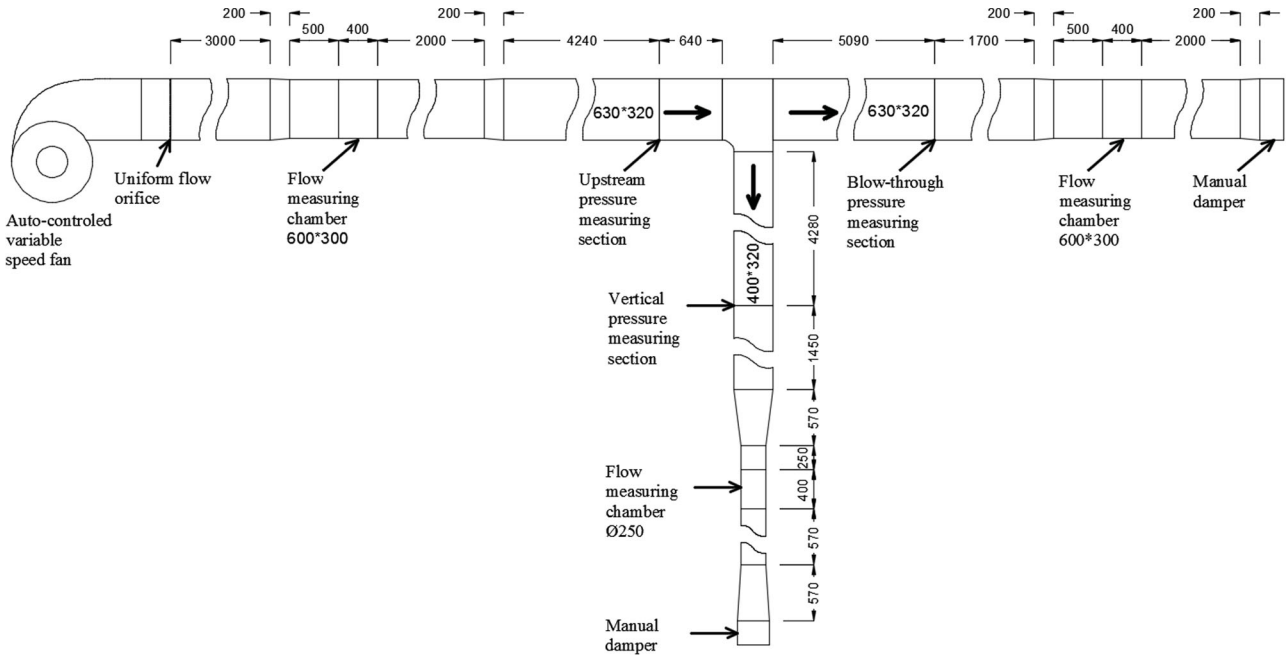

Figure 3. Diagrammatic drawing of junction resistance test apparatus.

The subscripts u, b and v refer to the pressure measuring section of upstream, blow-through and vertical branch respectively. $1/2\rho V^2$ refers to dynamic pressure and P_s the static pressure. And $\Delta P_{f,u}$,$\Delta P_{f,b}$, $\Delta P_{f,v}$ means the duct friction pressure loss of upstream duct, blow-through and vertical branch, respectively. It should be noted that the reason why the LPLCs are not calculated using the method from the ASHRAE Standard 120, where the dynamic pressure of the downstream section is used as the denominator, is that the downstream dynamic pressure could be very small for some relatively extreme conditions, such as a flow ratio of 0.1/0.9. Small variations in the measured data could introduce large differences in the LPLC value. However, the value of the upstream dynamic pressure, in contrast, is relatively larger and more stable during the measuring process. Therefore, to reduce errors, the above equations were applied. Although a comprehensive comparison for the LPLC calculation method used here against AHSRAE database is not presented here, the experiments are sufficient to support calibration of CFD parameters and the data points show a more obvious trend.

The duct friction pressure loss coefficient was calculated using the Moody equation (Moody 1947), as Equation (6), in which the roughness height of K was determined by a straight duct resistance experiment and Re as Equation (7). Then the fiction pressure loss is calculated using Darcy equation (ASHRAE 2009) as Equation (8).

$$\lambda = 0.0055\left[1 + (20,000\frac{K}{d} + \frac{10^6}{Re})^{1/3}\right], \quad (6)$$

$$Re = 66.4dV, \quad (7)$$

$$\Delta P_f = \lambda\frac{l}{d}(1/2\rho V^2). \quad (8)$$

Since the Moody equation was applied to the LPLC calculation for both the CFD and experimental results and the friction pressure loss and upstream dynamic pressure were almost the same, only the total pressure loss on both sides need to be compared to each other. For the vertical branch, the measured total pressure loss was obtained by summing the difference of the static and dynamic pressures between the upstream and downstream sections. For the blow-through, the static pressure difference is too small to be measured accurately. We used a Pitot tube and a differential pressure gauge with a high sensitivity to measure the total pressure difference at the centre of the sections.

On the other side of CFD simulation, the settings of meshing and CFD calculation were as follows:

- Meshing: Four layers of boundary mesh with 3 mm wide for the first layer; 20 mm of mesh size along the flow direction and 10 mm among the cross section and smaller mesh size applied at the junction.
- Boundary conditions: Velocity inlet with the same volume flow as in experiment; inlet turbulence defined in the mode of hydraulic diameter and turbulence intensity which is calculated as Equation (9); Outflow outlet; Wall roughness height set within $0.15 \sim 1$ mm and roughness constant within $0.5 \sim 1$.

$$\text{Turbulence intensity} = 0.16Re^{-0.125}. \quad (9)$$

Turbulence model: Standard $k - \varepsilon$ model.

- Convergence condition: $1e-3$ for continuity and $1e-6$ for other variables.
- SIMPLE pressure–velocity coupled algorithm and default scheme of ANSYS Fluent 14.0 for variable discretization.

Case design process for CFD calculation

Before case design, the dependent and independent variables should be determined. The LPLCs for the blow-through and vertical branch became the dependent variables. According to the influencing factors in some existing LPLC tables, we first chose the section area ratios AR_b and AR_v and the flow ratio FR_b as the independent variables. The subscripts b and v refer to the ratio of blow-through and the vertical branch to the upstream, respectively. In addition, since Shao and Riffat (1995) states that the Reynolds number *Re* also has an impact on the LPLC, we included the upstream inlet velocity V to reflect the influence of *Re*.

China's state and local construction departments have published a few manufacturing specification standards for duct fittings. In one of the local standards (DBJT05-104) (Building Standard Design Institute of Liaoning Province of China 1999), the section area ratio (AR) for a smooth tee junction should meet the following limits:

$$\begin{aligned} &1 \le AR_b + AR_v \le 1.16, \\ &AR_b \ge 0.5, \\ &AR_v \le 0.65. \end{aligned} \tag{10}$$

Based on the dimensional recommendations in the standard, six combinations of AR_b and AR_v were determined in total, as shown in Table 1. Since a linear constraint exists between AR_b and AR_v, we designed a tri-variable case set for each level of AR_b and used the multi-level uniform design table U_6 ($6^2 \times 2$) to arrange the cases, where AR_v was set in the corresponding two levels and FR_b and V in the six levels within [0.1, 0.9] and [4, 12], respectively, as listed in Table 2. The reason why the range of FR_b is [0.1,0.9] is that some branch flow may be very small during operation when the corresponding terminal damper is nearly closed. Then, the geometry models for the CFD calculation were constructed according to the values of AR_b and AR_v, and the boundary conditions were set according to the values of FR_b and V. Finally, the LPLCs for both the blow-through and vertical branches were calculated using Equation (4) and (5), where the total pressure loss is obtained from CFD and the friction pressure loss is calculated using Equation (6)–(8). Two decimal places of the LPLC results are reserved.

Table 1. Combinations of AR_b and AR_v.

AR_b	AR_v
0.5	0.5
	0.63
0.63	0.4
	0.5
0.8	0.25
	0.3

Table 2. Uniform design case set.

Case No.	AR_b	AR_v	FR_b	V (m/s)
1	0.50	0.5	0.1	5.6
2		0.63	0.26	8.8
3		0.5	0.42	12
4		0.63	0.58	4
5		0.5	0.74	7.2
6		0.63	0.9	10.4
7	0.63	0.4	0.1	5.6
8		0.5	0.26	8.8
9		0.4	0.42	12
10		0.5	0.58	4
11		0.4	0.74	7.2
12		0.5	0.9	10.4
13	0.80	0.25	0.1	5.6
14		0.3	0.26	8.8
15		0.25	0.42	12
16		0.3	0.58	4
17		0.25	0.74	7.2
18		0.3	0.9	10.4

PSO-FWSVR of LPLC data

After the CFD results for the LPLCs were obtained, the corresponding feature weighted support vector regression (FWSVR) model could be constructed. The feature weights and some parameters of FWSVR was optimized using PSO algorithm. Here presents some basics of the FWSVR and PSO algorithms.

The machine learning method of SVR is actually an application of support vector classification method by introducing the loss functions, which deals with the regression problems. The most popular loss function is the epsilon loss function proposed by Vapnik (1995). For a certain training set like $T = \{(x_1, y_1), (x_2, y_2) \ldots (x_i, y_i) \ldots\} \in (R^n \times R^1)$, where $x_i \in R^{1\times n}, y_i \in R, i = 1, 2 \ldots l$. Thus, the independent variable x_i is a multi-dimensional vector. Each dimension refers to an influencing factor, which is called the feature of x_i. SVR utilizes kernel function to map the data from the original data space to some high-dimensional feature space when nonlinear relationship exists between x_i and y_i. And the most popular kernel function is Gaussian radial basis kernel function as Equation (11) which satisfies the Mercer condition as Equation (12).

$$\varphi(x_i, x_j) = \exp(-\gamma ||x_i - x_j^2||), \tag{11}$$

$$k(x_i, x_j) = \varphi(x_i) \cdot \varphi(x_j). \tag{12}$$

When the correlation degree with y_i varies among the different features of x_i, applying the same feature weight to all of the features during regression can cause undesirable prediction accuracy. One can use a diagonal matrix of $A = \mathrm{diag}(\gamma_1, \gamma_2 \ldots \gamma_i \ldots), i = 1, 2 \ldots n,$ where $\gamma_i \in [0, 1]$ representing the weight of the i'th feature, to assign different weight to each feature. And the unknown parameters of the final feature weighted SVR function as Equation (13) are estimated by minimizing the following dual problem as Equation (14) and Equation (15), where C is the regularization parameter.

$$f(x) = \sum_{i=1}^{n} (a_i^* - a_i) K(Ax_i, Ax) + b, \tag{13}$$

$$\min \frac{1}{2} \sum_{i,j=1}^{n} (a_i - a_i^*)(a_j - a_j^*)(\varphi(Ax_i) \cdot \varphi(Ax_j)) + \sum_{i=1}^{n} a_i(\varepsilon - y_i) + \sum_{i=1}^{n} a_i^*(\varepsilon + y_i), \tag{14}$$

$$\text{s.t.} \begin{cases} \sum_{i=1}^{n} (a_i - a_i^*) = 0 \\ a_i, a_i^* \in [0, C] \end{cases}. \tag{15}$$

The prediction performance of the SVR is strongly affected by the selection of the regularization parameter C, the kernel function parameter γ and the loss function parameter ε. The K-fold cross validation (CV) method is usually used to determine the appropriate SVR parameters. For one combination of parameters, the K-fold CV method divides the training set into K groups, chooses one of them as the test set, uses the rest to train a SVR model and calculates the errors of this SVR model using the test set. This process is performed until every group has been used as the test set. The average test error for each time is called the CV error for the current parameter combination. The SVR training and K-fold CV process was performed using LIBSVM, a Matlab SVR toolbox developed by Chang and Lin (2011).

Heuristic algorithms are often used to efficiently find proper parameters. Among them, the PSO algorithm is a good choice because of their quick convergence and good optimization precision. The use of the PSO algorithm has been proposed by Kennedy and Eberhart (1995). In 1998, Shi and Eberhart (1998) introduced an inertia weight ω to improve the convergence performance. Since then, PSO with an inertia weight has gradually become the standard PSO algorithm. In the optimization process for the PSO, every particle flies in the solution space of the optimization problem. The position of each particle represents a potential solution. In addition to a position, a velocity is also assigned to each particle. During every iteration, the particles update their own velocities and positions, as defined in Equation (16) and (17). To balance the ability of local and global searching properly, dynamic inertia weight is often applied, meaning that ω changes during iterations. In this study, ω is determined from Equation (18).

$$v_i^{k+1} = \omega v_i^k + c_1 r_1 (p_i - z_i^k) + c_2 r_2 (p_g - z_i^k), \tag{16}$$

$$z_i^{k+1} = z_i^k + v_i^{k+1}, \tag{17}$$

$$\omega^k = \omega_{\max} - \frac{\omega_{\max} - \omega_{\min}}{\mathrm{iter}_{\max}} \times k, \tag{18}$$

where p_i represents the best position of the i'th particle, p_g represents the best position of the entire group, z_i^k is the position of the i'th particle during k'th iteration, c_1, c_2 are acceleration factors, r_1, r_2 are random numbers between [0, 1], ω^k is the inertia weight for the k'th iteration and $\mathrm{iter}_{\max}$ is defined as the maximum number of iterations.

Here, we used PSO with the linear dynamic inertia weight to simultaneously determine the SVR parameters of C and γ and the weights of each feature for the independent variables to build the PSO-FWSVR model of the LPLCs. The detailed modelling process is described by taking the vertical branch LPLC as an example, which is analogous to the modelling process for blow-through branch LPLC.

We chose the area ratios AR_b and AR_v, the upstream inlet velocity V and the velocity ratio (VR) of the vertical branch to the upstream duct VR_v as the features of the independent variable. So here $x_i = (\mathrm{AR}_b, \mathrm{AR}_v, \mathrm{VR}_v, V)$. The reason why VR_v was used instead of the flow ratio was that some researchers have mentioned that the correlation between the LPLC and VR exhibited more regularity than the correlation using the flow ratio, which has also been validated during trials. Therefore, the weight of VR_v was set to 1 and the weights of the others were altered by the PSO. So the position vector $z_i = (W_{\mathrm{AR}_b}, W_{\mathrm{AR}_b}, W_V, C, \gamma)$, where W means the feature weight. The CV error was used as the fitness function. Prior to regression, the values of VR_v and V were linearly normalized using Equation (19). Some other constants for the PSO and the alternation range of the optimization variables are shown in Table 3.

$$x_i' = \frac{x_i - x_{\min}}{x_{\max} - x_{\min}}. \tag{19}$$

Since SVR has a very strong ability of regression, it is common to use another entirely different dataset to test the prediction accuracy of the SVR model. Here we chose two sets of data to use as the test set. Group A (25 points) was the full permutation results of the LPLCs of a tee junction whose AR_b and AR_v were both set to 0.5 when FR_b and V were set in five levels each within their own range. This was used to test the model performance when predicting the LPLCs of a junction with a certain dimension for different combinations of FR_b and V. Group B (5 points) was the LPLC results of the junctions with the remaining five AR_b and AR_v combinations and random values for FR_b and V. This group was used to test the model performance for junctions with different dimensions. The prediction performance on the test set was evaluated using the mean square error (MSE), the correlation coefficient R^2 and the mean

Table 3. PSO constant and alternation range of optimization variables.

PSO constant				Alternation range of optimization variables		
(c_1, c_2)	$(\omega_{max}, \omega_{min})$	$iter_{max}$	Population size	Feature weight	C	γ
(2, 2)	(1.2, 0.4)	500	20	[0,1]	[0.1, 100]	[0.01, 10]

absolute percentage error (MAPE), as shown in Equation (20) and Equation (21):

$$\mathrm{MSE} = \frac{1}{n}\sum_{i=1}^{n} |\xi_{\mathrm{CFD},i} - \xi_{\mathrm{SVR},i}|^2, \tag{20}$$

$$\mathrm{MAPE} = \frac{1}{n}\sum_{i=1}^{n} \left| \frac{\xi_{\mathrm{CFD},i} - \xi_{\mathrm{SVR},i}}{\xi_{\mathrm{CFD,ave}}} \right| \times 100\%, \tag{21}$$

where $\xi_{\mathrm{CFD,ave}}$ is the mean value of the CFD LPLCs of the test set.

Comparison with the traditional LPLC models

First, we compared the results from both the polynomial model and PSO-FWSVR model to the CFD results to verify the improvement in accuracy when calculating the LPLC of an individual junction. Here, the constant value model was removed since it keeps the LPLC unchanged. To build the polynomial model, we performed a univariate cubic polynomial regression for both the blow-through and vertical branch LPLCs with the same training set using the VR as the independent variable.

Then, we transitioned to the system level and modelled a simple duct system with three outlets connected by several straight ducts and two tee junctions and driven by a constant speed fan using the Simulink platform, as shown in Figure 4. The three tee junction LPLC models were used one by one. Here, three dampers with hydraulic diameters of 315, 200 and 200 mm were placed at outlets A, B and C, respectively. The rated flows were 3000 and 2000 m^3/h. The relationship between flow, opening and resistance is described as a 2D table, from which the pressure loss for each combination of flow and damper opening could be looked up. The data were provided by a damper manufacturer. Then, the capacity of the fan was determined according to the total flow summed from all of the outlets and the corresponding pressure loss from the ductwork. The fan flow and static pressure curves were defined as quadratic polynomial functions. For the ducts, the friction was determined using the Moody equation. Since it is only a demo to demonstrate the influence of LPLC model to system operation condition, the length of each duct was tuned to achieve a balanced flow between the branches at the rated condition for simplicity. For the constant model, the tee junction LPLC value at the rated flow condition was chosen to be kept constant during the simulations. Here, the rated LPLC value was set to be the same as that from the PSO-FWSVR model.

The simulation period was set to be 200 s. During the simulation, the opening of the damper at outlet B was defined as a ramp function, as shown in Figure 4, which started to decrease at 50 s from 100% to 30% over the following 150 s. Dampers A and C were kept 100% open

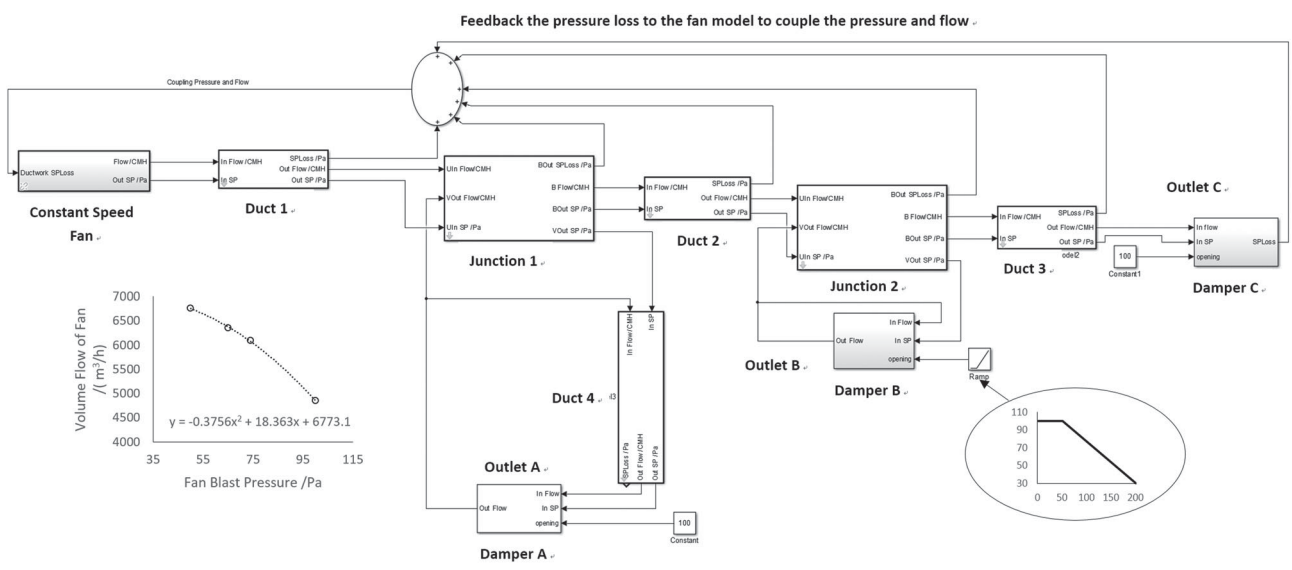

Figure 4. Demonstration of simple duct system driven by constant speed fan.

throughout the simulation process. The flow conditions and the LPLCs of the two junctions were monitored for comparison.

Results and discussion

Calibration of CFD roughness parameter

After several rounds of trials and errors, the total pressure loss results for a roughness height of 0.7 mm (which is larger than the 0.15 mm ideal roughness height for galvanized sheet iron) and a roughness constant of 0.8 were found to be in best agreement with the experimental data. As shown in Figure 5, the mean absolute error for the blow-through branch is 10.6% and is 4.07% for the vertical branch. After roughness parameter calibration, the pressure loss results from the CFD are very close to the measured data. This roughness parameter combination was used in all of the other CFD calculations.

LPLCs results of PSO-FWSVR model

We first trained the PSO-FWSVR$_{UD}$ model for the vertical branch LPLC using the 18-point uniform design results.

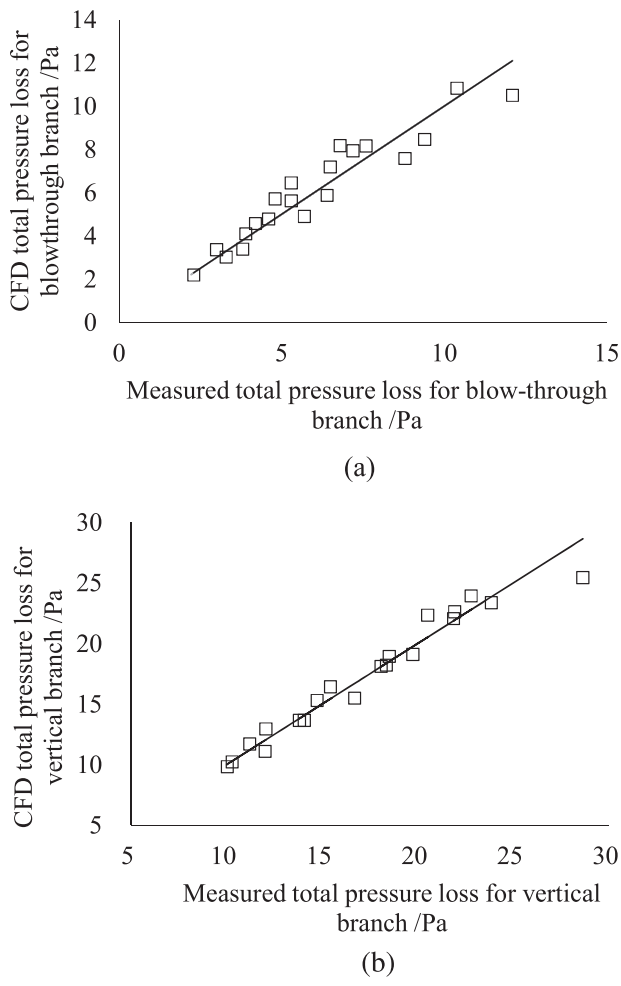

Figure 5. Comparison between measured total pressure loss and CFD results:(a) blow-through branch, (b) vertical branch.

Table 4. Final feature weights, SVR parameters and MSE, R^2 and MAPE of PSO-FWSVR$_{UD}$ for vertical branch LPLC.

Feature weights	(C, γ)	MSE	R^2	MAPE/%
(1, 0, 1, 0.018)	(100, 1.647)	0.0570	0.9728	16.84

Note: the figures in (1, 0, 1, 0.018) represent the weights of AR$_b$, AR$_v$, VR$_v$ and V successively.

The final optimized feature weights, SVR parameters and results of the MSE, R^2 and MAPE are listed in Table 4.

From Table 4, the predicted R^2 is as high as 0.973. The weight of AR$_v$ is altered to 0 by the PSO, meaning that the influence from AR$_v$ could be neglected based on this set of training data. One way to explain this is that the VR is actually the result of the flow ratio divided by the AR so that the influence of the AR is reflected to some extent in the VR. In the meantime, the weight of the upstream velocity V is also remarkably reduced to 0.018. To understand this, we examined the distribution of the vertical branch LPLCs of test set group A, as shown in Figure 6 (a). The vertical branch LPLCs have a polynomial relationship with VR$_v$

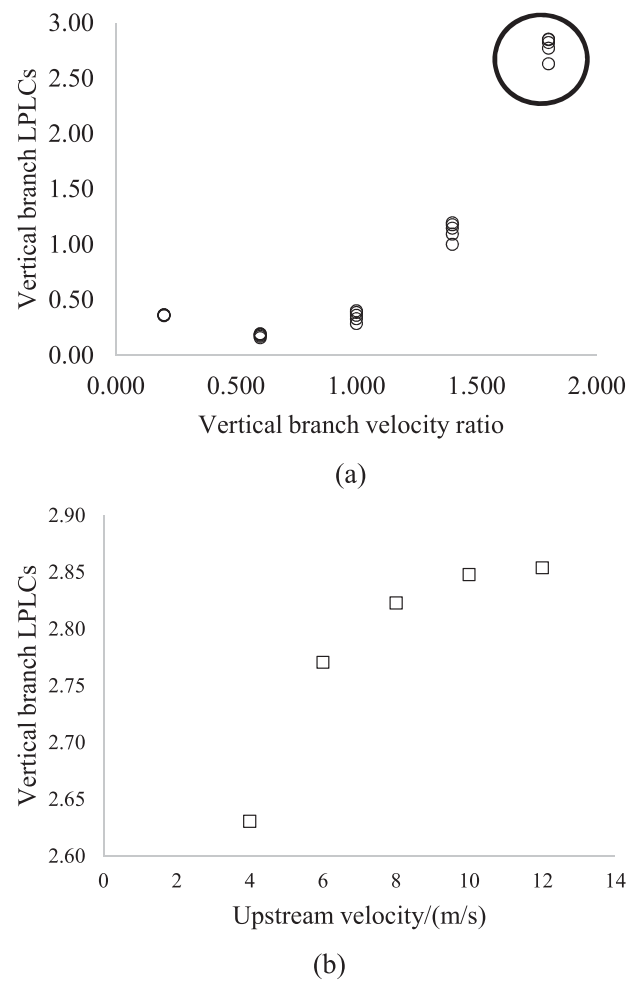

Figure 6. Distribution of LPLCs of group A on the dimension of velocity ratio and upstream velocity. (Note: The five points in (b) are those from the circle in (a).)

on a macro level, which is consistent with previous conclusions. Only over a relatively small range do the LPLCs vary with the upstream velocity for a certain level of VR, as shown in Figure 6 (b). Therefore, the weight of the upstream velocity is small.

However, one fact that cannot be ignored is that although the R^2 of PSO-FWSVR$_{UD}$ is very high, the MAPE is 16.84%, which is still too high to accept. More importantly, the feature weight of AR$_v$ is set as 0, which is physically unreasonable. To address this, we first observed the distribution of the relative errors in the LPLCs, as shown in Figure 7. Most of the large errors are associated with the small LPLCs. When we zoom in the small LPLC zone as shown in Figure 8, we can see that the original PSO-FWSVR$_{UD}$ cannot reflect the true trend for the LPLCs along with upstream velocity, which happens to be the opposite. Since the weight of the upstream velocity is significantly reduced, an alternation of the feature weight may result. To eliminate this possibility, we constructed a PSO-SVR$_{UD}$ model with equal feature weights using the same 18-points training set. The results of this examination for the small LPLC region are also shown in Figure 8. The trend from this examination is even stranger. After this potential reason was excluded, we believed that this error may be caused by the small size of the training set. Although the uniform design method guarantees the uniformity of the data points in the sample space, fewer points lead to longer distances between each other. The SVR has an extremely strong fitting capability. As a result, the functional relationship between data points may be twisted. From Figure 6 (a), we can see that the LPLC variations caused by the upstream velocity are not the same for the different velocity ratios. The larger the LPLCs, the stronger the influence from the upstream velocity. Therefore, the feature weights may be different when the LPLCs fall into zones of different values. However, since only one set of feature weights could be used for training, to help the PSO to determine an appropriate feature weight, we decided to supplement more data points with small LPLCs to feed

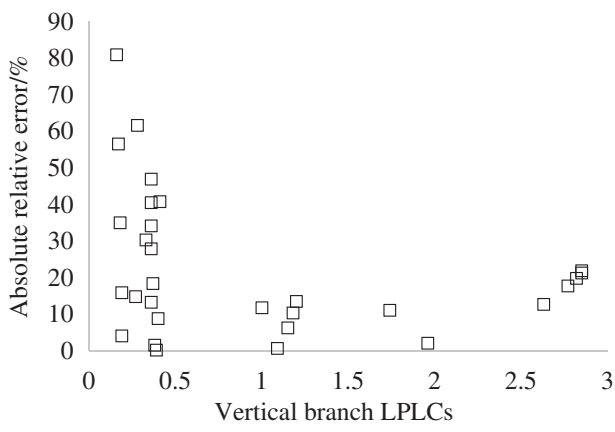

Figure 7. Distribution of relative error on test set.

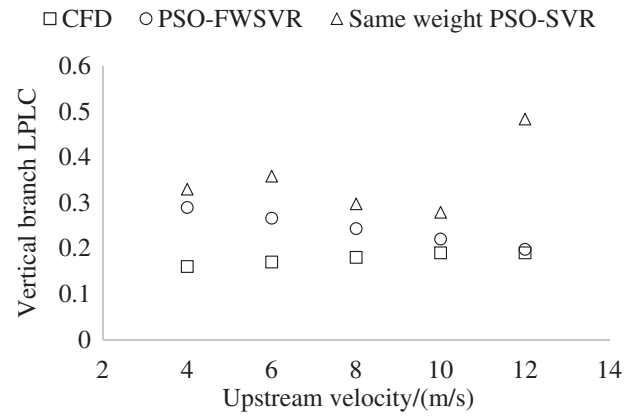

Figure 8. Comparison between CFD results and SVR predictions among the points with big error.

the model with more information on this region. The same amount of points from the larger value zone was also used in the training set to ensure balance.

Since the LPLCs are macroscopically influenced by the VR, we must determine for which VR the LPLCs are relatively small or large for the junctions for different combinations of AR$_b$ and AR$_v$. Here, we used the same weight PSO-SVR$_{UD}$ model to predict the LPLCs for an 8 m/s upstream velocity and a flow ratio from 0.1 to 0.9 for every junction with the AR$_b$ and AR$_v$ values listed in Table 1. We assumed that the macroscopic trend in the predicted results was reproducible, regardless of the fact that every single LPLC value may be inaccurate. The preliminary prediction results are shown in Figure 9. For a junction of a certain dimension, the largest vertical branch LPLCs appear when flow ratio is 0.1 and the smallest appear near $0.7 \sim 0.8$. Finally, we performed three supplemental CFD calculations for every junction with the upstream velocity set at 4, 8 and 12 m/s and the flow ratio set to 0.1 for the large LPLC value zone and also performed another three calculations for the small value zone. Therefore, for the entire set of six types of junctions, there are $6 \times 6 = 36$ supplemental data points.

Then, the 36 supplemental points together with the original 18 uniform design points were used to train the PSO-FWSVR$_{UD+Sup}$ model. The final feature weights, SVR parameters and accuracy indices are listed in Table 5. Using the supplemental points, the MSE and R^2 improve and, more importantly, the MAPE decreases considerably from 16.84% to 2.76%. We can also find that the optimized feature weights are changed. The weight of AR$_v$ is no longer zero and the weight of AR$_b$ decreases from 1 to 0.583. The influence of the upstream velocity also increases. From the variation of MAPE, we can infer that the targeted supplemental points have a positive effect on determining the proper feature weights and corresponding SVR parameters with which the PSO-FWSVR model can adequately fit all the test points throughout the available range.

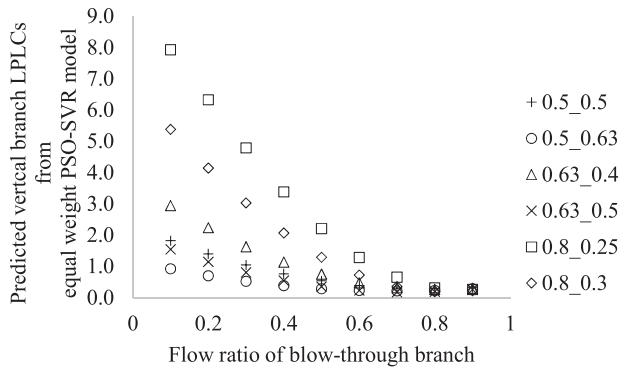

Figure 9. Preliminary prediction results of vertical branch LPLCs from equal weight PSO-SVR model. (Note: the figures like 0.63_0.5 in the legend are the values of AR_b and AR_v successively).

Table 5. Final feature weights, SVR parameters and accuracy indexes of $PSO\text{-}FWSVR_{UD+Sup}$ for vertical branch LPLC.

Feature weights	(C, γ)	MSE	R^2	MAPE/%
(0.583, 0.375, 1, 0.072)	(100, 9.965)	0.0016	0.9982	2.76

Note: the figures of (0.583, 0.375, 1, 0.072) have the same meaning as the notation of Table 2.

Table 6. Final feature weights, SVR parameters and accuracy indexes of $PSO\text{-}FWSVR_{UD+Sup}$ for blow-through branch LPLC.

Feature weights	(C, γ)	MSE	R^2	MAPE/%
(0.164, 0.623, 1, 0.193)	(100, 1.637)	0.00016	0.9993	2.46

Note: the figures of (0.164, 0.623, 1, 0.193) represent the weights of AR_b, AR_v, VR_b (velocity ratio of blow-through branch to upstream) and V successively.

The PSO-FWSVR model for blow-through branch LPLC was built using the same procedure as that for the vertical branch. The corresponding results of the PSO-FWSVR model are listed in Table 6, which shows a consistently good prediction performance.

Comparison with the traditional LPLC models

Individual junction level comparison

The MAPEs of the vertical and blow-through branch LPLC results from the polynomial model are 27.93% and 11.25%, respectively. The comparison results are shown in Figure 10. The prediction results from the PSO-FWSVR model are closer to the CFD results for almost every test data point compared. Using the VR of the downstream branch to the upstream branch as the only independent variable to predict the LPLC is insufficient to reflect the highly nonlinear relationship that the LPLC has with its influencing factors. The vertical branch LPLC suffers more significantly than blow-through branch.

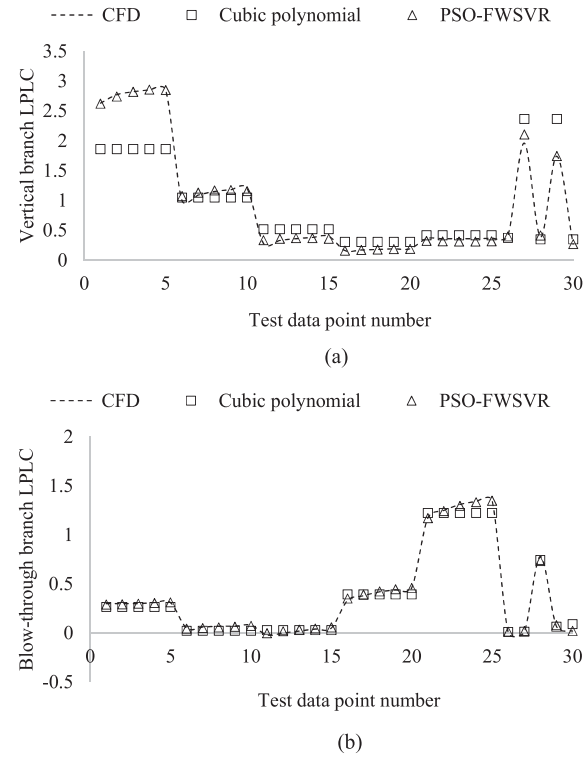

Figure 10. LPLC prediction performance comparison between cubic polynomial model and PSO-FWSVR model.

System-level comparison

On the system-level comparison, the results of the system total flow using different LPLC models are shown in Figure 11. We treat the results from the PSO-FWSVR model as the baseline since it is the most complex and accurate LPLC model for an individual junction. Compared with the baseline, the polynomial results have a stable bias, which is less than 150 m^3/h, whereas the results from the constant value model start to deviate from the baseline after 50 s and end up with a bias greater than 700 m^3/h, which is nearly 15% of the baseline total flow.

Let us take a detailed look at the flow conditions and corresponding LPLCs at the two junctions for these three

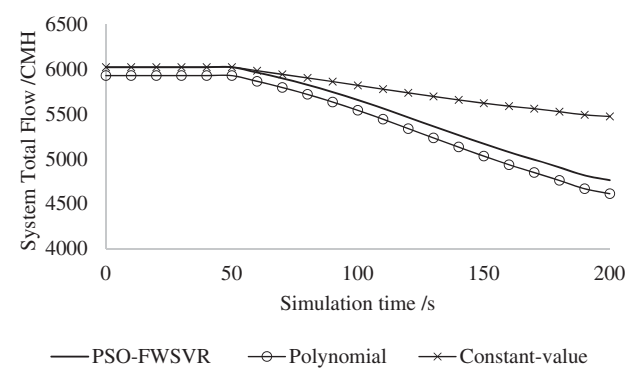

Figure 11. System total flow comparison among three LPLC models.

cases and attempt to determine any noticeable differences. First we compare the results from the polynomial model with the baseline. Figures 12 and 13 show the flow conditions and LPLC results for junction 1, respectively. When damper B starts closing, more air is forced into outlet A and the total flow decreases. In Figure 12, the biggest difference between the polynomial result and the baseline is that the increasing rate of the polynomial vertical flow of junction 1 is not as rapid as the baseline. The bias of the polynomial vertical flow from the baseline is approximately $-150\,m^3/h$, which is 5% of the baseline vertical flow. This is explained by the corresponding change of LPLCs in Figure 13. The vertical LPLC from the polynomial model increases faster than the baseline and its relative error increases from 20.2% at the beginning to 59.6% at the end of the simulation because the polynomial model only considers the influence of the VR and ignores the upstream velocity. The increasing vertical VR causes the vertical LPLC increases, whereas the decreasing upstream velocity causes it to decrease. For the blow-through flow, the difference between the polynomial result and the baseline is completely neglected because the value of the blow-through LPLC is very small and the bias of the polynomial blow-through LPLC is stable throughout the simulation. The corresponding figures are not explained further as the difference in the flow condition and the LPLCs of junction 2 determined via the polynomial model and the baseline are very small. Therefore, we see that using the polynomial LPLC model and neglecting the influence of the upstream velocity can cause a large error in the LPLC initially and then cause a different change rate in the corresponding branch flow. However, the influence of this causality becomes less significant when the value of LPLC is small, such as less than 0.1.

Then, we compared the results of the constant value model with the baseline, as shown in Figures 14–17.

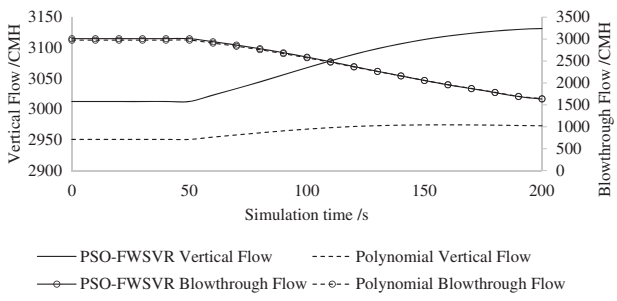

Figure 12. Comparison of flow condition of junction 1 between polynomial and the baseline model.

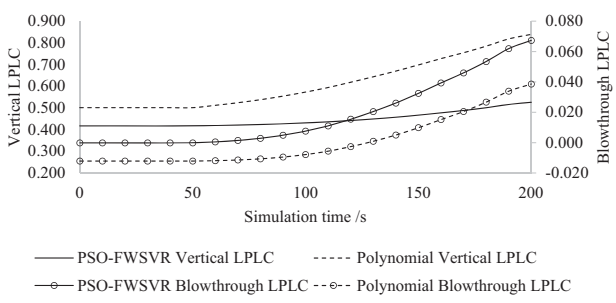

Figure 13. Comparison of LPLCs of junction 1 between polynomial and the baseline model.

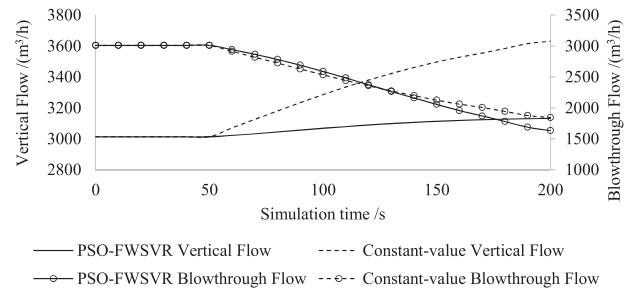

Figure 14. Comparison of flow condition of junction 1 between constant value and the baseline model.

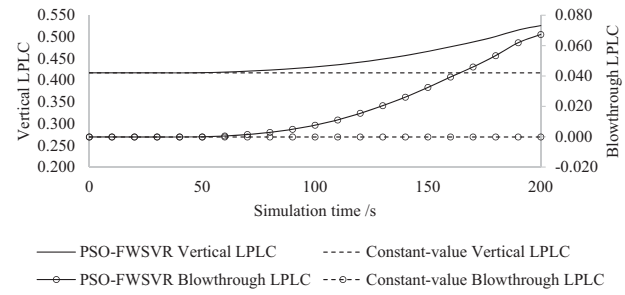

Figure 15. Comparison of LPLCs of junction 1 between constant value and the baseline model.

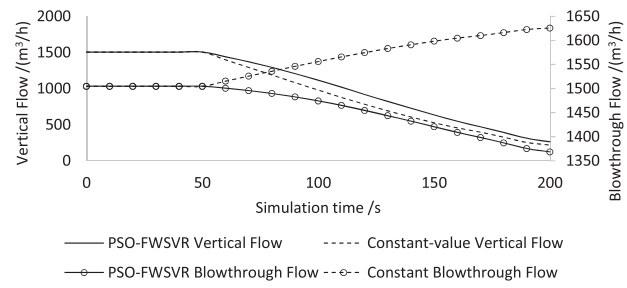

Figure 16. Comparison of flow condition of junction 2 between constant value and the baseline model.

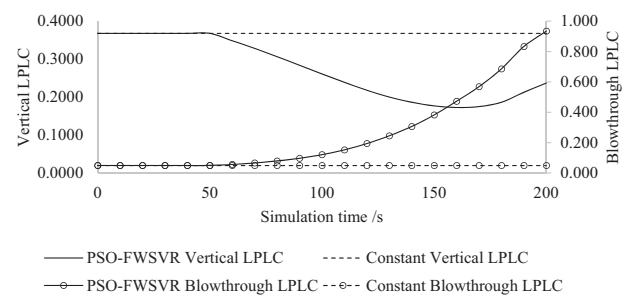

Figure 17. Comparison of LPLCs of junction 2 between constant value and the baseline model.

Table 7. Comprehensive dataset of LPLCs for diverging smooth tee junctions generated by PSO-FWSVR.

Geometric configuration	Flow ratio[b]		Inlet veocity/(m/s) 4	5	6	7	8	9	10	11	12
0.5_0.5[a]	0.1	*B*[c]	0.289	0.291	0.293	0.295	0.298	0.301	0.305	0.308	0.313
		V[c]	2.621	2.686	2.741	2.785	2.819	2.843	2.855	2.858	2.849
	0.2	*B*	0.154	0.155	0.157	0.159	0.161	0.164	0.168	0.171	0.175
		V	1.759	1.807	1.847	1.878	1.902	1.916	1.922	1.920	1.909
	0.3	*B*	0.045	0.047	0.050	0.054	0.057	0.061	0.065	0.069	0.073
		V	1.073	1.106	1.132	1.152	1.165	1.173	1.173	1.167	1.155
	0.4	*B*	− 0.015	− 0.010	− 0.004	0.001	0.007	0.012	0.017	0.022	0.027
		V	0.608	0.628	0.645	0.657	0.664	0.667	0.665	0.658	0.647
	0.5	*B*	− 0.001	0.008	0.017	0.025	0.033	0.040	0.047	0.052	0.058
		V	0.333	0.346	0.357	0.365	0.369	0.371	0.369	0.365	0.357
	0.6	*B*	0.115	0.129	0.143	0.155	0.166	0.175	0.183	0.190	0.195
		V	0.200	0.210	0.217	0.223	0.228	0.230	0.231	0.230	0.228
	0.7	*B*	0.352	0.373	0.392	0.409	0.424	0.436	0.446	0.453	0.458
		V	0.159	0.165	0.170	0.175	0.179	0.182	0.185	0.187	0.189
	0.8	*B*	0.715	0.744	0.770	0.793	0.812	0.828	0.841	0.849	0.854
		V	0.196	0.198	0.200	0.202	0.204	0.207	0.209	0.212	0.215
	0.9	*B*	1.171	1.209	1.243	1.272	1.297	1.317	1.333	1.343	1.349
		V	0.323	0.319	0.316	0.314	0.312	0.312	0.312	0.313	0.315
0.5_0.63	0.1	*B*	0.275	0.276	0.278	0.281	0.284	0.287	0.291	0.295	0.300
		V	0.619	0.663	0.701	0.734	0.761	0.783	0.798	0.807	0.811
	0.2	*B*	0.141	0.142	0.144	0.147	0.150	0.153	0.157	0.161	0.166
		V	0.405	0.439	0.468	0.493	0.513	0.528	0.539	0.545	0.546
	0.3	*B*	0.044	0.046	0.049	0.053	0.056	0.061	0.065	0.069	0.074
		V	0.301	0.327	0.349	0.368	0.383	0.394	0.402	0.406	0.406
	0.4	*B*	− 0.002	0.003	0.008	0.013	0.018	0.023	0.028	0.033	0.038
		V	0.269	0.288	0.305	0.320	0.332	0.341	0.347	0.350	0.351
	0.5	*B*	0.021	0.029	0.036	0.044	0.050	0.056	0.062	0.067	0.071
		V	0.274	0.289	0.302	0.313	0.322	0.330	0.335	0.339	0.340
	0.6	*B*	0.131	0.144	0.155	0.165	0.174	0.182	0.188	0.193	0.196
		V	0.297	0.308	0.317	0.325	0.333	0.339	0.343	0.347	0.349
	0.7	*B*	0.345	0.363	0.379	0.393	0.405	0.415	0.422	0.428	0.430
		V	0.339	0.344	0.350	0.354	0.359	0.363	0.366	0.369	0.371
	0.8	*B*	0.667	0.692	0.714	0.734	0.750	0.763	0.772	0.778	0.781
		V	0.410	0.411	0.411	0.412	0.412	0.413	0.414	0.415	0.416
	0.9	*B*	1.071	1.105	1.134	1.160	1.181	1.198	1.210	1.218	1.221
		V	0.526	0.520	0.516	0.512	0.508	0.505	0.502	0.500	0.499
0.63_0.4	0.1	*B*	0.311	0.312	0.314	0.316	0.318	0.320	0.323	0.326	0.329
		V	3.471	3.549	3.615	3.668	3.709	3.736	3.751	3.752	3.741
	0.2	*B*	0.201	0.201	0.202	0.203	0.205	0.207	0.209	0.211	0.214
		V	2.603	2.669	2.723	2.767	2.800	2.821	2.830	2.828	2.815
	0.3	*B*	0.100	0.100	0.101	0.103	0.105	0.107	0.109	0.112	0.114
		V	1.727	1.776	1.816	1.846	1.868	1.880	1.883	1.877	1.861
	0.4	*B*	0.017	0.019	0.022	0.024	0.027	0.030	0.033	0.037	0.040
		V	1.037	1.069	1.095	1.114	1.126	1.131	1.128	1.119	1.103
	0.5	*B*	− 0.035	− 0.030	− 0.026	− 0.021	− 0.016	− 0.012	− 0.007	− 0.003	0.001
		V	0.598	0.619	0.636	0.647	0.654	0.656	0.652	0.644	0.631
	0.6	*B*	− 0.039	− 0.031	− 0.023	− 0.016	− 0.009	− 0.002	0.004	0.009	0.014
		V	0.373	0.388	0.400	0.410	0.416	0.420	0.420	0.417	0.411
	0.7	*B*	0.022	0.034	0.046	0.057	0.067	0.075	0.083	0.090	0.096
		V	0.269	0.281	0.292	0.301	0.309	0.315	0.320	0.323	0.324
	0.8	*B*	0.161	0.179	0.195	0.209	0.222	0.234	0.244	0.251	0.257
		V	0.254	0.262	0.269	0.276	0.283	0.290	0.296	0.301	0.307
	0.9	*B*	0.389	0.412	0.434	0.453	0.470	0.484	0.496	0.505	0.511
		V	0.374	0.374	0.375	0.376	0.378	0.381	0.383	0.387	0.390
0.63_0.5	0.1	*B*	0.311	0.312	0.314	0.316	0.319	0.322	0.325	0.329	0.333
		V	1.201	1.261	1.313	1.356	1.391	1.417	1.434	1.442	1.441
	0.2	*B*	0.196	0.197	0.198	0.200	0.202	0.204	0.207	0.210	0.214
		V	0.756	0.802	0.842	0.875	0.901	0.919	0.931	0.934	0.931
	0.3	*B*	0.094	0.095	0.097	0.099	0.101	0.104	0.107	0.111	0.115

(*Continued*).

Table 7. Continued.

Geometric configuration	Flow ratio[b]		Inlet veocity/(m/s) 4	5	6	7	8	9	10	11	12
		V	0.491	0.526	0.555	0.579	0.598	0.610	0.617	0.617	0.612
	0.4	*B*	0.015	0.018	0.021	0.024	0.027	0.031	0.035	0.038	0.043
		V	0.375	0.401	0.424	0.442	0.455	0.464	0.468	0.468	0.463
	0.5	*B*	− 0.032	− 0.027	− 0.023	− 0.018	− 0.013	− 0.008	− 0.003	0.002	0.006
		V	0.340	0.360	0.378	0.392	0.404	0.412	0.416	0.417	0.415
	0.6	*B*	− 0.033	− 0.026	− 0.018	− 0.011	− 0.004	0.002	0.008	0.014	0.018
		V	0.329	0.346	0.360	0.372	0.382	0.390	0.396	0.399	0.400
	0.7	*B*	0.026	0.038	0.049	0.059	0.068	0.076	0.083	0.089	0.094
		V	0.331	0.342	0.352	0.362	0.370	0.377	0.383	0.387	0.391
	0.8	*B*	0.157	0.173	0.188	0.201	0.213	0.224	0.232	0.239	0.244
		V	0.376	0.381	0.385	0.390	0.394	0.398	0.402	0.405	0.408
	0.9	*B*	0.369	0.391	0.411	0.428	0.443	0.456	0.466	0.474	0.479
		V	0.508	0.506	0.504	0.502	0.501	0.500	0.499	0.499	0.499
0.8_0.25	0.1	*B*	0.311	0.311	0.311	0.312	0.313	0.314	0.315	0.317	0.319
		V	8.531	8.611	8.678	8.731	8.771	8.796	8.808	8.805	8.789
	0.2	*B*	0.235	0.233	0.233	0.232	0.232	0.232	0.232	0.233	0.234
		V	6.319	6.401	6.471	6.528	6.572	6.603	6.621	6.626	6.617
	0.3	*B*	0.158	0.156	0.155	0.155	0.154	0.154	0.154	0.154	0.155
		V	4.325	4.399	4.462	4.513	4.553	4.580	4.595	4.597	4.588
	0.4	*B*	0.083	0.083	0.082	0.081	0.081	0.081	0.082	0.082	0.083
		V	3.066	3.125	3.173	3.211	3.238	3.253	3.258	3.251	3.233
	0.5	*B*	0.018	0.019	0.019	0.020	0.021	0.022	0.023	0.024	0.026
		V	2.008	2.045	2.074	2.094	2.105	2.107	2.100	2.084	2.059
	0.6	*B*	− 0.029	− 0.027	− 0.024	− 0.022	− 0.019	− 0.017	− 0.014	− 0.012	− 0.009
		V	1.058	1.076	1.088	1.095	1.095	1.090	1.078	1.061	1.037
	0.7	*B*	− 0.051	− 0.046	− 0.041	− 0.036	− 0.031	− 0.027	− 0.022	− 0.019	− 0.015
		V	0.527	0.540	0.549	0.555	0.558	0.557	0.554	0.547	0.537
	0.8	*B*	− 0.036	− 0.027	− 0.019	− 0.012	− 0.004	0.002	0.008	0.014	0.018
		V	0.351	0.364	0.377	0.388	0.399	0.408	0.416	0.423	0.429
	0.9	*B*	0.026	0.038	0.050	0.061	0.071	0.080	0.088	0.095	0.101
		V	0.382	0.388	0.394	0.402	0.409	0.417	0.425	0.433	0.442
0.8_0.3	0.1	*B*	0.319	0.319	0.320	0.321	0.322	0.324	0.326	0.328	0.330
		V	5.021	5.100	5.168	5.224	5.268	5.300	5.319	5.326	5.320
	0.2	*B*	0.238	0.237	0.237	0.237	0.237	0.238	0.239	0.240	0.241
		V	3.568	3.639	3.700	3.749	3.787	3.814	3.829	3.832	3.824
	0.3	*B*	0.158	0.157	0.156	0.156	0.156	0.156	0.157	0.158	0.159
		V	2.563	2.621	2.670	2.708	2.736	2.753	2.760	2.756	2.742
	0.4	*B*	0.081	0.080	0.080	0.080	0.081	0.081	0.082	0.083	0.085
		V	1.703	1.744	1.777	1.801	1.816	1.823	1.821	1.810	1.790
	0.5	*B*	0.014	0.015	0.016	0.017	0.019	0.020	0.022	0.024	0.026
		V	1.000	1.024	1.042	1.054	1.060	1.059	1.051	1.037	1.017
	0.6	*B*	− 0.035	− 0.032	− 0.029	− 0.026	− 0.023	− 0.020	− 0.017	− 0.014	− 0.011
		V	0.603	0.619	0.631	0.638	0.642	0.641	0.636	0.627	0.614
	0.7	*B*	− 0.057	− 0.052	− 0.046	− 0.041	− 0.036	− 0.031	− 0.027	− 0.023	− 0.019
		V	0.455	0.470	0.482	0.493	0.501	0.507	0.510	0.511	0.510
	0.8	*B*	− 0.043	− 0.035	− 0.026	− 0.018	− 0.011	− 0.004	0.002	0.007	0.012
		V	0.401	0.413	0.425	0.437	0.447	0.457	0.466	0.474	0.481
	0.9	*B*	0.017	0.029	0.041	0.052	0.062	0.071	0.079	0.086	0.092
		V	0.463	0.467	0.470	0.475	0.479	0.484	0.489	0.495	0.500

[a]The figure like 0.5_0.5 in the column of geometric configuration means the junction whose AR_b and AR_v are 0.5 and 0.5 successively.
[b]The flow ratio is the proportion of blow-through flow rate in the entire flow rate.
[c]*B*, *V* means the value of LPLC is for the blow-through and vertical branch, respectively.

Figures 14 and 15 show the flow conditions and LPLC results for junction 1, and Figures 16 and 17 provide the flow conditions and LPLC results for junction 2. In Figures 14 and 15, the result is similar, as the result from the polynomial model shows that the main difference exists in the vertical FR. However, in this case, the vertical flow from the constant value model increases faster than the baseline result, and its final bias is 500 m^3/h, which is 16% of the baseline vertical flow and is bigger than the bias from the polynomial model. In Figure 15, the

constant value model keeps the LPLC value unchanged, which is copied from the baseline value at the beginning of simulation, and ends with an error of -20.7%. Then, as seen from Figures 16 and 17, the difference is more significant. The blow-through flow of the constant value model increases, whereas the baseline blow-through flow decreases, which is in two different directions. The reason why the baseline blow-through flow decreases is that the baseline blow-through LPLC increases greatly and becomes large enough to prevent more air from being forced into outlet C. Therefore, we see that using the constant value LPLC model results in a bigger deviation than the polynomial model, and additionally, under some circumstances, it may lead to completely opposite variation of flow condition.

From the comparisons and analyses of the results from the three models at the system level, we first conclude that the constant value LPLC model is essentially unusable since the variation from the fixed value of the rated condition can be very large, resulting in an error greater than 10% of the system total flow and a completely different variation for the branch flow. Therefore, if one needs to reflect the mutual influence of adjacent terminal dampers correctly, the constant value LPLC model should not be used. With regard to the polynomial model, it appears that the difference between it and the baseline is not very large, with only a 5% error of the branch flow in the above demonstration. However, if we define specific situations, the difference may be essential. We know that the branch flow and the pressure loss along this branch are mutually dependent based on the fan curve. The pressure losses from each branch all equal to the blast pressure of the fan if we assume that the outlet pressure of the damper equals the inlet pressure of the fan, as in the above demonstration. The extent to which the LPLC model of the junction influences the branch flow condition is shown by the relative magnitude of the local pressure loss at the junction compared with the fan blast pressure. As seen in Figure 13, the error in the LPLC using the polynomial model may be as large as nearly 60%, meaning that the local pressure loss at the junction also has an error of 60% from its actual value. Therefore, if the simulated fan is a one with a low blast pressure and a relatively large flow, deviations in the flow condition using polynomial LPLC model may be more significant. Additionally, if the simulated system demands high precision control, such as a precisely controlled constant temperature and humidity conditioner, the error from the polynomial model is unacceptable.

The baseline model (PSO-FWSVR) development process is difficult, but it could be easily deployed and quickly calculated during simulations. If the simulation platform is not compatible with the LIBSVM code, it could be used to generate a look-up table with enough levels of independent variables, as Table 7, which is still more accurate than the other two models.

Conclusion

This study used the PSO-FWSVR method to build a new LPLC model for a smooth diverging tee junction. Then, the accuracy of the PSO-FWSVR and polynomial models was compared at the individual junction level. Finally, a model of a small air-side system was built to demonstrate the functionality of the two models and the constant value LPLC model at the system level. The main conclusions are:

(1) For LPLC model development, it is efficient to use a uniform design method for the CFD case arrangement and adopt the PSO-FWSVR method for data fitting. In this way, we can obtain an accurate LPLC model with relatively fewer CFD calculations.
(2) The PSO-FWSVR model can accurately calculate the LPLC for junctions of different dimensions under different upstream velocity and flow allocation conditions, which is much better than the polynomial model for an individual junction.
(3) At the system level, the constant value assumption for the LPLCs of junctions is too simple to reflect the variation of the air-side system condition correctly. The polynomial LPLC model using the VR as its uni-independent variable may be used to simulate the most common HVAC air-side systems, but more care should be taken when simulating precision-controlled systems.

Nomenclature

ρ	Density of air (kg/m^3)
$1/2\rho V^2$	Dynamic pressure (Pa)
ΔP_f	Friction pressure loss (Pa)
K	Roughness height (m)
D, d	Hydraulic diameter (m)
AR	Area ratio of the downstream to upstream section
FR	Flow rate ratio of the downstream to upstream section
VR	Velocity ratio of the downstream to upstream section
V	Upstream inlet velocity (m/s)
λ	Friction pressure loss coefficient
l	Length of straight duct (m)
C	Regularization parameter of SVR
Γ	Constant in Gaussian radial basis kernel function of SVR
c_1, c_2	Accelerating factors for local and global searching abilities of PSO
ω^k	Inertia weight for the k'th iteration of PSO
ξ	Value of LPLC
W	Weight of certain feature of independent variable

Subscripts

u	Upstream branch
b	Blow-through branch
v	Vertical branch
CFD	The LPLC value calculated by CFD
SVR	The LPLC value predicted by SVR
ave	Average value
UD	Using only the dataset of uniform design cases
UD + Sup	Using the dataset of both uniform design cases and the supplemental cases

References

AHSRAE. 2008. *ANSI/AHSRAE Standard 120-2008, Method of Testing to Determine Flow Resistance of HVAC Ducts and Fittings*. Atlanta: American Society of Heating, Air-Conditioning and Refrigeration Engineers.

ASHRAE. 2009. *2009 ASHRAE Handbook – Fundamentals (SI).* Atlanta: American Society of Heating, Air-Conditioning and Refrigeration Engineers.

Building Standard Design Institute of Liaoning Province of China. 1999. *HVAC Component Installation (Part 1) Manufacture and Connection of Ductwork*. Shenyang: Liaoning Standard Press. (In Chinese).

Chang, C. C., and C. J. Lin. 2011. "LIBSVM: A Library for Support Vector Machines." *ACM Transactions on Intelligent Systems & Technology* 2 (3): 389–396.

Chen, Y., and S. Treado. 2014. "Development of a Simulation Platform Based on Dynamic Models for HVAC Control Analysis." *Energy and Buildings* 68: 376–386.

China Academy of Building Research. 1978. *China National Technical Chart of Ventilation Ductwork and Fittings*. Beijing: China Architecture & Building Press. (In Chinese).

Fang, K. T., and D. Lin. 2008. *Uniform Design in Computer and Physical Experiments*. Edited by H. Tsubaki, K. Nishina and S. Yamada. Tokyo: Springer.

Fang, K. T., D. Lin, P. Winker, and Y. Zhang. 2000. "Uniform Design: Theory and Application." *Technometrics* 42 (3): 237–248.

Gan, G. H., and S. B. Riffat. 2000. "Numerical Determination of Energy Losses at Duct Junctions." *Applied Energy* 67 (3): 331–340.

Idel'chik, I. E. 1986. *Handbook of Hydraulic Resistance*. 3rd ed. Edited by M. O. Steinberg and translated by G. R. Malyavskaya and O. G. Martynenko. New York: Hemisphere.

Kennedy, J., and R. Eberhart. 1995. "Particle Swarm Optimization." *IEEE International Conference on Neural Networks Proceedings* 4: 1942–1948.

Lin, S., Z. Lee, S. Chen, and T. Tseng. 2008. "Parameter Determination of Support Vector Machine and Feature Selection Using Simulated Annealing Approach." *Applied Soft Computing* 8 (4): 1505–1512.

Liu, W., Z. Long, and Q. Chen. 2012. "A Procedure for Predicting Pressure Loss Coefficients of Duct Fittings Using Computational Fluid Dynamics (RP-1493)." *HVAC&R Research* 18 (6): 1168–1181.

Liu, M., H. Peng, and J. Zhang. 2012. "Research on Simulation Math Model of Pressure-Independent VAV Air-Conditioning System." *Building Energy & Environment* 31 (03): 8–12. (In Chinese).

Miller, Donald S. 1971. *Internal Flow: A Guide to Losses in Pipe and Duct Systems*. Cranfield: British Hydromechanics Research Association.

Moody, M. L. 1947. "An Approximate Formula for Pipe Friction Factors." *Transactions of ASME* 69: 1005–1006.

Mumma, S., T. Mahank, and Y. Ke. 1997. "Close Coupled Ductwork Fitting Pressure Drop." *HVAC&R Research* 3 (2): 158–177.

Mumma, S. A., T. A. Mahank, and Y. Ke. 1998. "Analytical Determination of Duct Fitting Loss-Coefficients." *Applied Energy* 61 (4): 229–247.

Niu, D., and Y. Guo. 2010. "An Improved PSO for Parameter Determination and Feature Selection of SVR and its Application in STLF." *Journal of Multiple-Valued Logic and Soft Computing* 16 (6SI): 567–584.

Shao, L., and B. Riffat. 1995. "CFD for Prediction of K-Factors of Duct Fittings." *International Journal of Energy Research* 19 (1): 89–93.

Shi, Y., and R. Eberhart. 1998. "Modified Particle Swarm Optimizer." *IEEE International Conference on Evolutionary Computation Proceedings* 6: 69–73.

Vapnik, V. 1995. *The Nature of Statistical Learning*. Berlin: Springer.

Wetter, M. 2009. "Modelica-based Modelling and Simulation to Support Research and Development in Building Energy and Control Systems." *Journal of Building Performance Simulation* 2 (2): 143–161.